Reactivity of the C−X (X = F, Cl, Br, and I) Bond Activation in CX_4 by an Iridium(I) Complex from a Theoretical Viewpoint

Ming-Der Su* and San-Yan Chu*

Contribution from the Department of Chemistry, National Tsing Hua University, Hsinchu 30043, Taiwan, Republic of China

Received August 31, 1998. Revised Manuscript Received October 16, 1998

Abstract: Complete geometry optimizations were carried out using density functional theory to study potential energy surfaces of the transition-metal complex insertions into carbon−halogen bonds. The *trans*-Ir(Cl)$(PH_3)_2$ + CX_4 (X = F, Cl, Br, I) systems are the subject of the present study. Three different reaction mechanisms are proposed and are as follows: (I) oxidative insertion (OxIn) of *trans*-Ir(Cl)$(PH_3)_2$ into the C−X bond, (ii) radical mechanisms proceeding via single electron transfer (SET), and (iii) backside S_N2 substitution mechanisms. The results of B3LYP/LANL2DZ calculations suggest the following: (a) For oxidative addition of 14-electron T-shaped ML_3 complexes to saturated C−X bonds the order of reactivity is I > Br > Cl ≫ F, whether collision conditions exist or not. (b) The ease of oxidative insertion increases with increasing halogen electronegativity. For the heavier halogens, especially idoine, OxIn and SET reaction pathways are in competition. (c) In the competition of the S_N2 path with OxIn and SET processes, the former has the highest energy requirement and is therefore the least energetically favorable path in all cases in the gas phase. Further, the reaction pathway cannot be determined for the singlet transition states. The problem has been solved by computing the intrinsic reaction coordinate (IRC). The IRC results have demonstrated that the transition state corresponds to a CX_3 fragment abstraction, rather than the backside S_N2 substitution. Furthermore, a configuration mixing model based on the work of Pross and Shaik is used to rationalize the computational results. It is demonstrated that both the σ(C−X) → σ^*(C−X) triplet excitation energy of halocarbons and the halogen lone-pair repulsions play a decisive role in determining the dominant reaction pathways (i.e., OxIn or SET).

I. Introduction

Halocarbons have been used extensively in agriculture, industry, home products, etc., and as their utility has expanded, their deleterious properties have become manifest and their role as contaminants of the environment has created considerable concern.[1,2] Much attention has been paid to the remediation of the damage that has been caused by the use of halocarbons. Finding a potential catalyst which enables the activation of carbon−halogen bonds is thus extremely desirable. Although the activation of C−H and C−C bonds by transition-metal complexes is well-known,[3] examples of C−X (X = F, Cl, Br, and I) activation are rare as a result of the chemical inertness of C−X bonds;[4,5] particularly little is known about the mechanism of C−X activation. Systematically experimental and theoretical studies of C−X activation pathways have not, to the best of our knowledge, been undertaken.[6] In addition, mechanistic studies of C−X bond activation reactions have been difficult because of low quantum yields, which make it impossible to observe reactive intermediates.[4] Theory therefore plays an important role in the investigation of the mechanisms of such oxidative addition reactions, which are indispensable for the achievement of real understanding of the reaction mechanism, but which often cannot be realized experimentally.

Three basic mechanisms had previously been proposed for the oxidative addition of halocarbons to transition-metal complexes. A conventional proposal was for a concerted reaction wherein the metal inserts into the C−X bond (OxIn).[7] Here the σ-bonding electrons in the C−X bond can donate to a vacant orbital on the metal; retrodonation (from a filled d_{xz} or d_{yz}; vide infra) into the σ^* orbital on the halocarbon would cause bond making and breaking (see eq 1; [M] stands for the transition-metal complex). An alternative proposal was a radical mechanism proceeding via a single electron transfer (SET) and either a halogen atom or a CX_3 group abstraction (see eq 2).[6] Further,

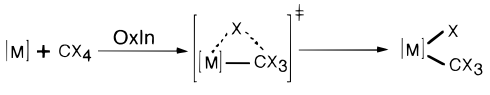

(1)

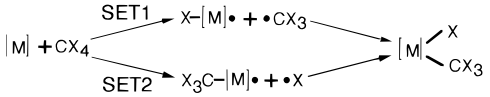

(2)

an S_N2-type mechanism was also considered, in which the metal center acts as a nucleophile utilizing the nonbonding electrons

(1) (a) Crutzen, P. J. *Angew. Chem., Int. Ed. Engl.* **1996**, *35*, 1758. (b) Molina, M. J. *Ibid.* **1996**, *35*, 1778. (c) Rowland, F. S. *Ibid.* **1996**, *35*, 1787.

(2) (a) McElroy, M. E.; Salawitch, R. J.; Wofsy, S. C.; Logan, J. A. *Nature (London)* **1986**, *321*, 755. (b) Saunders, G. C. *Angew. Chem., Int. Ed. Engl.* **1996**, *35*, 2615.

(3) (a) Crabtree, R. H. In *Activation and Functionalization of Alkanes*; Davies, J. A., Ed.; VCH: New York, 1990; p 69. (b) Crabtree, R. H. *Angew. Chem., Int. Ed. Engl.* **1993**, *32*, 789. (c) Schroder, D.; Schwarz, H. *Ibid.* **1995**, *34*, 1937. (d) Amdtsen, B. A.; Bergman, R. G.; Mobley, T. A.; Peterson, T. H. *Acc. Chem. Res.* **1995**, *28*, 154.

(4) Crabtree, R. H. *The Organometallic Chemistry of The Transition Metals*; John Wiley & Sons: New York, 1994.

(5) The bond energy for C−X (X = F, Cl, Br, and I) is 116, 78.2, 68, and 51 kcal/mol, respectively. See: Huheey, J. E.; Keiter, E. A.; Keiter, R. L. *Inorganic Chemistry*, 4th ed.; HarperCollins College Publishers: New York, 1993.

10.1021/ja9831148 CCC: $18.00
Published on Web 01/22/1999

in the d_{xz} or d_{yz} orbital (see eq 3). For OxIn and S_N2 reactions,

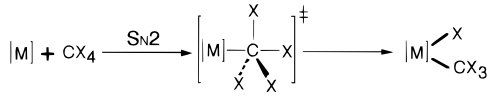

(3)

these two pathways should be readily distinguishable considering the stereochemistry at the carbon center in CX_4: the former requires retention at the reacting carbon atom, whereas the latter requires inversion. In contrast, the SET reaction would result in a complete loss of stereospecificity at carbon. Surprisingly none of these proposals seem to have been studied theoretically, with the exception of the density functional theory (DFT) study of the model reaction system Pd + CH_3Cl.[6] Thus, a detailed theoretical study of C−X oxidative additions to coordinatively unsaturated metal fragments is proposed to investigate the reaction pathways and to clarify the metal−halogen−carbon bonding interactions. Moreover, a better understanding of the thermodynamic and kinetic aspects of such oxidative additions may shed some light on optimal design of further related synthesis and catalytic processes.

It is the purpose of this paper to investigate a series of such reactions. We hereafter present a DFT study of the reaction

$$\textit{trans}\text{-Ir(Cl)(PH}_3)_2 + \text{X}-\text{CX}_3 \rightarrow \textit{trans}\text{-Ir(Cl)(PH}_3)_2(\text{X})(\text{CX}_3) \quad (4)$$

That is, we consider theoretically the reaction paths of a model oxidative addition of CX_4 to the coordinatively unsaturated d^8 complex of the type *trans*-Ir(Cl)$(PH_3)_2$, where X = F, Cl, Br, and I. The present work is the second of a series of papers concerned with DFT studies of the reaction mechanisms of oxidative addition of X−CX_3 and X−CH_3 (X = halogen) to a transition-metal complex.[8] Choosing eq 4 as a model system for oxidative addition of halocarbons is of particular interest for several reasons. First, in the previous study,[8] we have investigated the potential energy surface for C−F bond activation in CH_3F by coordinatively unsaturated *trans*-M(X)$(PH_3)_2$, where M = Rh and Ir and X = CH_3, H, and Cl. We have found that this model reaction actually has a low activation energy, especially for the *trans*-Ir(Cl)$(PH_3)_2$ complex. It is thus reasonable to predict that this complex should also easily activate other C−X (X = Cl, Br, and I) bonds, since the C−F bond is found to have the highest bond energy in the series of carbon−halogen bonds.[5] Second, it has been previously noted that iridium complexes are more prone to undergo single-electron-transfer reactions than their rhodium analogues (vide infra).[9] Moreover, the variations in X should reveal the eletronic influence of the halides on reactivity. Finally, organic reactions involving halocarbons exhibit considerable mechanistic variety; thus, eq 4 should be a favorable case for determining whether more than one mechanism might be operative for oxidative additions. We anticipate that the results obtained in this work may allow one to predict the reaction pathway for some known and/or as yet unknown systems.

The order of this paper is as follows. After the Introduction and the electronic structures of the model systems, we present in the third section the calculational results of eqs 1−3 using eq 4 as a model system. From those results various questions arise that require a rationalization, which are presented in section IV. Section V contains brief concluding remarks. Details of the calculations are given in the Appendix.

II. Electronic Structure of the ML_3 + CX_4 Model System

We first consider the electronic structure of the 14-electron T-shaped *trans*-Ir(Cl)$(PH_3)_2$ + CX_4 model system. The electronic characteristics of *trans*-Ir(Cl)$(PH_3)_2$ and CX_4 have been previously discussed and need no additional comments.[10] The main relevant molecular orbitals between the two fragments *trans*-Ir(Cl)$(PH_3)_2$ and CX_4 are shown in **1**. In the case of **1a**,

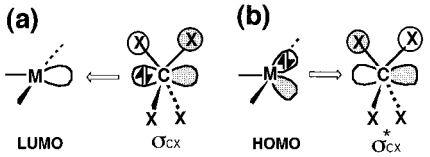

1

the LUMO on the metal center is the empty s/p/d hybrid orbital pointing toward the vacant site of *trans*-Ir(Cl)$(PH_3)_2$, into which the C−X σ orbital of a halocarbon can donate electrons. This electron donation accompanied by back-donation from the HOMO to the C−X σ^* orbital achieves C−X bond activation (see **1b**). The net molecular event involved in the insertion of the *trans*-Ir(Cl)$(PH_3)_2$ complex into a C−X σ bond of CX_4 is the formation of new metal−carbon and metal−halogen σ bonds, accompanied by the breaking of the carbon−halogen σ bond. This is a typical example of an oxidative addition reaction between a transition-metal complex and a X−CX_3 moiety.[8] The supporting calculational results are detailed below.

Before the calculational results are analyzed, it has to be pointed out that the ground state of *trans*-Ir(Cl)$(PH_3)_2$ was calculated to be the triplet state, the closed shell singlet state calculated to be 4.6 kcal/mol higher in energy.[8] This implies that the *trans*-Ir(Cl)$(PH_3)_2$ reactant in a triplet state might insert into the saturated C−X bond via a diradical mechanism. Nevertheless, as noted previously,[11] the spin−orbit coupling matrix element is directly proportional to the atomic number of an atom. Thus, whenever a reactant contains a heavy atom center (such as a transition metal) which is not necessarily directly involved in the reaction, a strong spin−orbit coupling may exist. In other words, the system, via the agency of a heavy atom, can enhance the probability of triplet−singlet radiationless decay through coupling of spin and orbital angular momenta. Additionally, as mentioned above, the DFT calculations suggest that the excitation energy from the triplet ground state to the first singlet state for the *trans*-Ir(Cl)$(PH_3)_2$ fragment is quite small (−4.6 kcal/mol). Hence, for these two reasons, the transition from the triplet to the singlet state would be easy, even if the triplet *trans*-Ir(Cl)$(PH_3)_2$ took part in the reaction

(6) Bickelhaupt, F. M.; Ziegler, T.; Schleyer, P. v. R. *Organometallics* **1995**, 14, 2288.
(7) Pearson, R. G.; Muir, W. R. *J. Am. Chem. Soc.* **1970**, *92*, 5519.
(8) Su, M.-D.; Chu, S.-Y. *J. Am. Chem. Soc.* **1997**, *119*, 10178.
(9) Chanon, M. *Bull. Soc. Chim. Fr.* **1982**, II-197.

(10) (a) Albright, T. A.; Burdett, J. K.; Whangbo, M. H. *Orbital Interaction in Chemistry*; Wiley: New York, 1985; p 339. (b) Su, M.-D. *Mol. Phys.* **1993**, *80*, 1223. (c) Su, M.-D. *Mol. Phys.* **1994**, *82*, 567.
(11) (a) Su, M.-D. *Chem. Phys. Lett.* **1995**, *237*, 317. (b) Su, M.-D. *J. Org. Chem.* **1995**, *60*, 6621. (c) Su, M.-D. *Tetrahedron* **1995**, *51*, 5871. (d) Su, M.-D. *Tetrahedron* **1995**, *51*, 12109. (e) Su, M.-D. *J. Phys. Chem.* **1996**, *100*, 4339. (f) Su, M.-D. *Chem. Phys.* **1996**, *205*, 277. (g) Su, M.-D. *J. Org. Chem.* **1996**, *61*, 3080.
(12) Indeed, our DFT calculations have shown that, for instance, in the SET2 case the triplet transition state of *trans*-Ir(Cl)$(PH_3)_2$ + CF_4 is 44.4 kcal/mol higher in energy than the corresponding singlet transition state (i.e., **SET2-TS-F** in Figure 1). In other words, this strongly indicates that the reaction of *trans*-Ir(Cl)$(PH_3)_2$ with CX_4 via SET should proceed on the singlet surface. Furthermore, it has been reported that singlet CH_2 reacts via abstraction with a C−Cl bond. For more detail sees: Roth, H. D. *Acc. Chem. Res.* **1977**, *10*, 85.

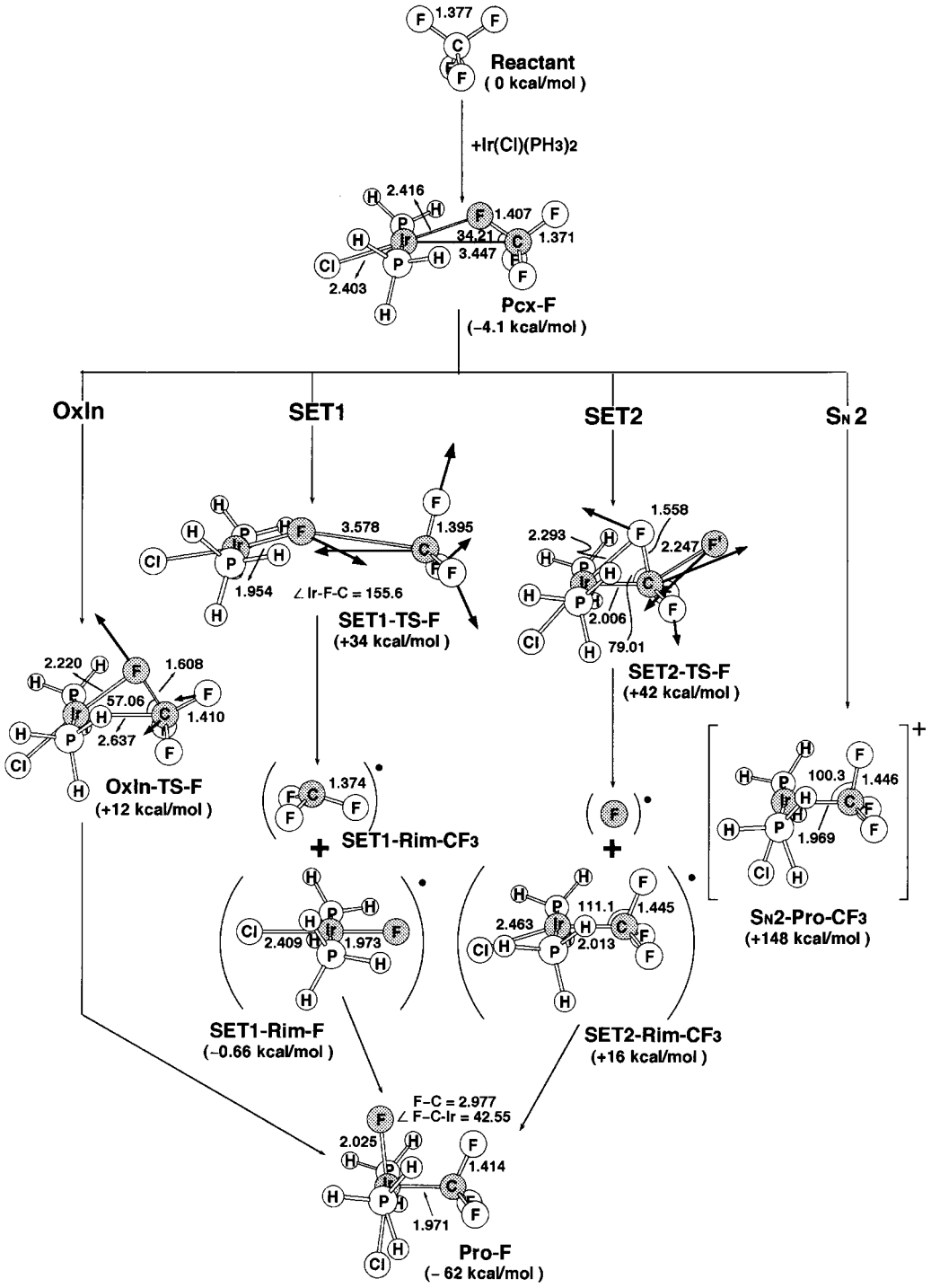

Figure 1. B3LYP/LANL2DZ optimized geometries (Å and deg) for stationary points of the *trans*-$Ir(Cl)(PH_3)_2 + CF_4$ reaction system. Values in parentheses are the relative energies at the B3LYP/LANL2DZ level. The heavy arrows indicate the main atomic motions in the transition-state eigenvector.

scheme.[12] Consequently, it is reaonable to conclude that the oxidative addition reactions should proceed on the singlet surface, even if the reactants start from the triplet state. We shall therefore focus on the singlet surface in what follows.

III. Results and Discussion

The optimized geometries calculated at the B3LYP/LANL2DZ level of theory involving reactants (**Rea**), precursor complexes (**Pcx**), transition states (**TS**), radical intermediates (**Rim**), and products (**Pro**) for the three kinds of reaction mechanisms described earlier are collected in Figures 1−4 for CF_4, CCl_4, CBr_4, and CI_4, respectively. For convenience, we have also given the energies relative to the two reactant molecules, i.e., *trans*-$Ir(Cl)(PH_3)_2 + CX_4$ (X = F, Cl, Br, and I). Relative energies for various reaction mechanisms are summarized in Table 1. To simplify the comparisons and to emphasize the trends, the calculated heats of reaction and the individual barrier heights are also listed in Table 1.

1. Mechanism for Oxidative Insertions. Let us first consider the oxidative insertion of *trans*-$Ir(Cl)(PH_3)_2$ to $X-CX_3$ (eq 1, OxIn). The corresponding reaction energy profiles for CX_4 (X = F, Cl, Br, and I) are given in Figure 5.

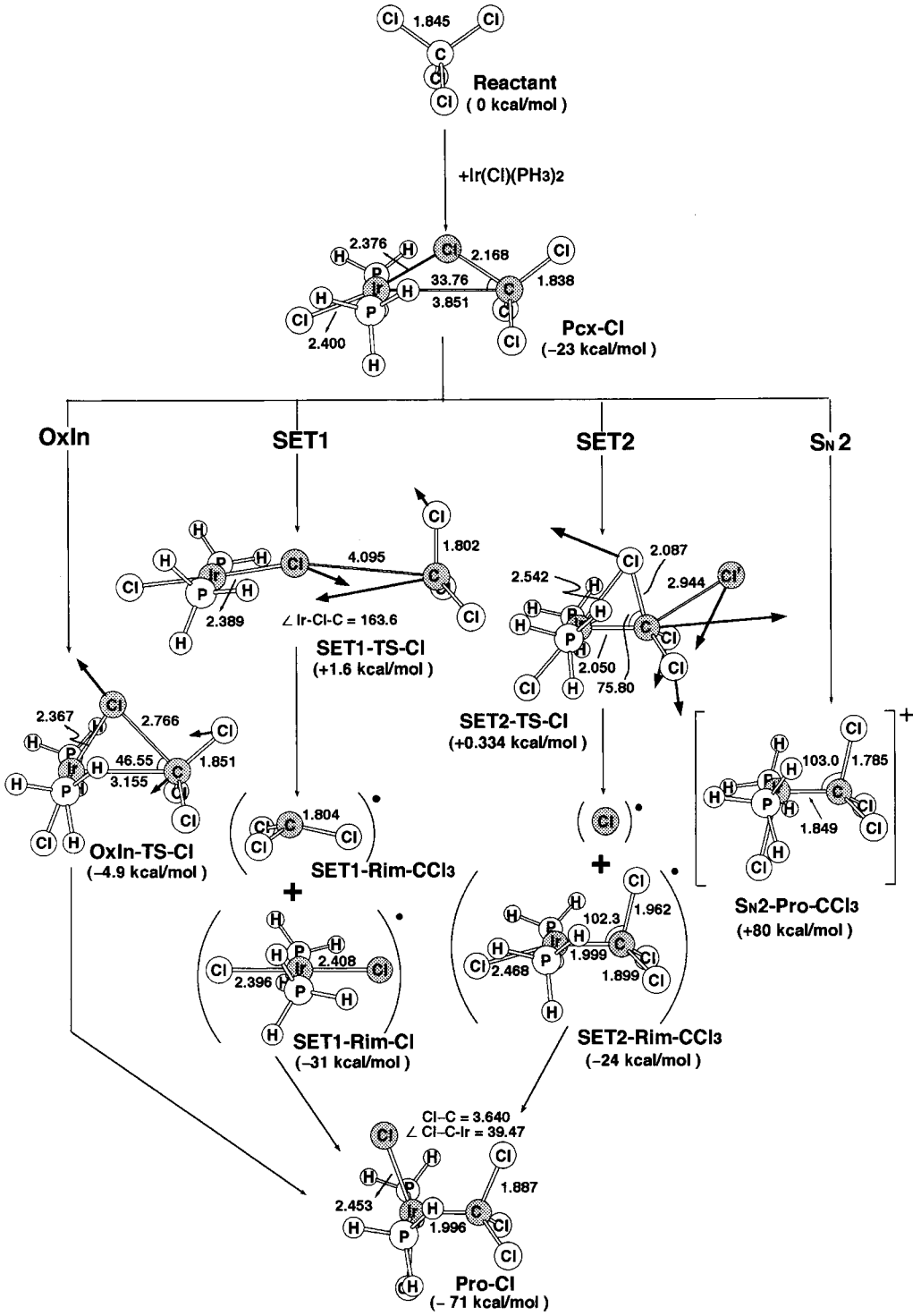

Figure 2. B3LYP/LANL2DZ optimized geometries (Å and deg) for stationary points of the *trans*-Ir(Cl)$(PH_3)_2$ + CCl_4 reaction system. Values in parentheses are the relative energies at the B3LYP/LANL2DZ level. The heavy arrows indicate the main atomic motions in the transition-state eigenvector.

Some interesting conclusions can be drawn from Figures 1−5 and Table 1. First, the precursor complexes (**Pcx-F**, **Pcx-Cl**, **Pcx-Br,** and **Pcx-I**) all display very similar Ir···(CX_4) bonding characteristics, and the monomer geometries are essentially unperturbed. The tetrahalomethane ligand is coordinated to Ir in an η^2 fashion via one Ir−C and one Ir−X σ bond with the X−C−X plane nearly orthogonal to the *trans*-Ir(Cl)$(PH_3)_2$ coordination plane. In addition, the distance between the carbon and the migrating halogen in the CX_4 moiety, for the precursor complexes studied here, is elongated, i.e., 1.407 Å (F), 2.168 Å (Cl), 2.297 Å (Br), and 2.417 Å (I), compared to 1.377 Å (F), 1.845 Å (Cl), 2.028 Å (Br), and 2.224 Å (I) for isolated CX_4. Moreover, the DFT results of Figures 1−4 show that the calculated bond distances for the Ir···C contacts increase on going from 3.447 Å (CF_4) to 3.851 Å (CCl_4) to 3.967 Å (CBr_4) to 4.100 Å (CI_4). Namely, the heavy halogen substitution causes a large increase in the distance between *trans*-Ir(Cl)$(PH_3)_2$ and CX_4. This finding can be explained in terms of the expected atom size of the halogen atom X, which should increase as X changes from F down to I.

The optimized transition-state structures (**OxIn-TS-F**, **OxIn-TS-Cl**, **OxIn-TS-Br**, and **OxIn-TS-I**) along with the calculated

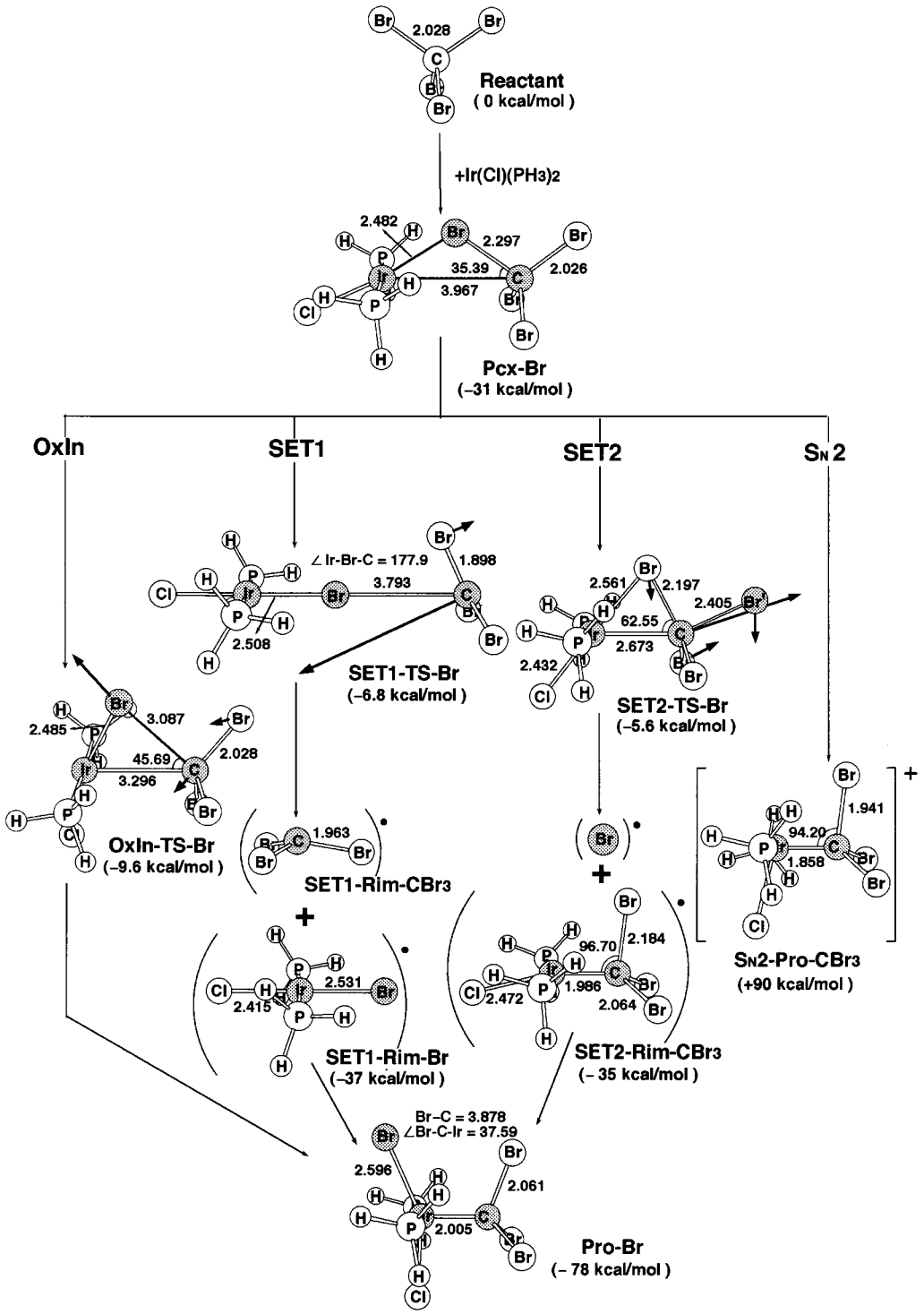

Figure 3. B3LYP/LANL2DZ optimized geometries (Å and deg) for stationary points of the *trans*-Ir(Cl)$(PH_3)_2$ + CBr_4 reaction system. Values in parentheses are the relative energies at the B3LYP/LANL2DZ level. The heavy arrows indicate the main atomic motions in the transition-state eigenvector.

transition vectors for the four oxidative insertions are shown in Figures 1−4, respectively. The arrows in the figures illustrate the directions in which the atoms move in the normal coordinate corresponding to the imaginary frequency. Examination of the single imaginary frequency for each transition state (329i cm^{-1} for **OxIn-TS-F**, 150i cm^{-1} for **OxIn-TS-Cl**, 87i cm^{-1} for **OxIn-TS-Br**, and 114i cm^{-1} for **OxIn-TS-I**) provides excellent confirmation of the concept of the insertion process. The vibrational motion for oxidative additions of CX_4 to *trans*-Ir(Cl)$(PH_3)_2$ involves the bond forming between iridium and carbon in concert with C−X bond breaking and halogen transfer to the adjacent iridium atom. Indeed, the primary similarity among those transition states is the three-center pattern involving iridium, carbon, and halogen atoms. It is noteworthy that such characteristic three-center transition states are quite analogous to mechanisms observed for oxidative additions of C−H bonds

(13) (a) Su, M.-D.; Chu, S.-Y. *Organometallics* **1997**, *16*, 1621. (b) Su, M.-D.; Chu, S.-Y. *J. Am. Chem. Soc.* **1997**, 119, 5373. (c) Su, M.-D.; Chu, S.-Y. *J. Phys. Chem.* **1997**, *101*, 6798. (d) Su, M.-D.; Chu, S.-Y. *Chem. Phys. Lett.* **1998**, *282*, 25. (e) Su, M.-D.; Chu, S.-Y. *Inorg. Chem.* **1998**, *37*, 3400.

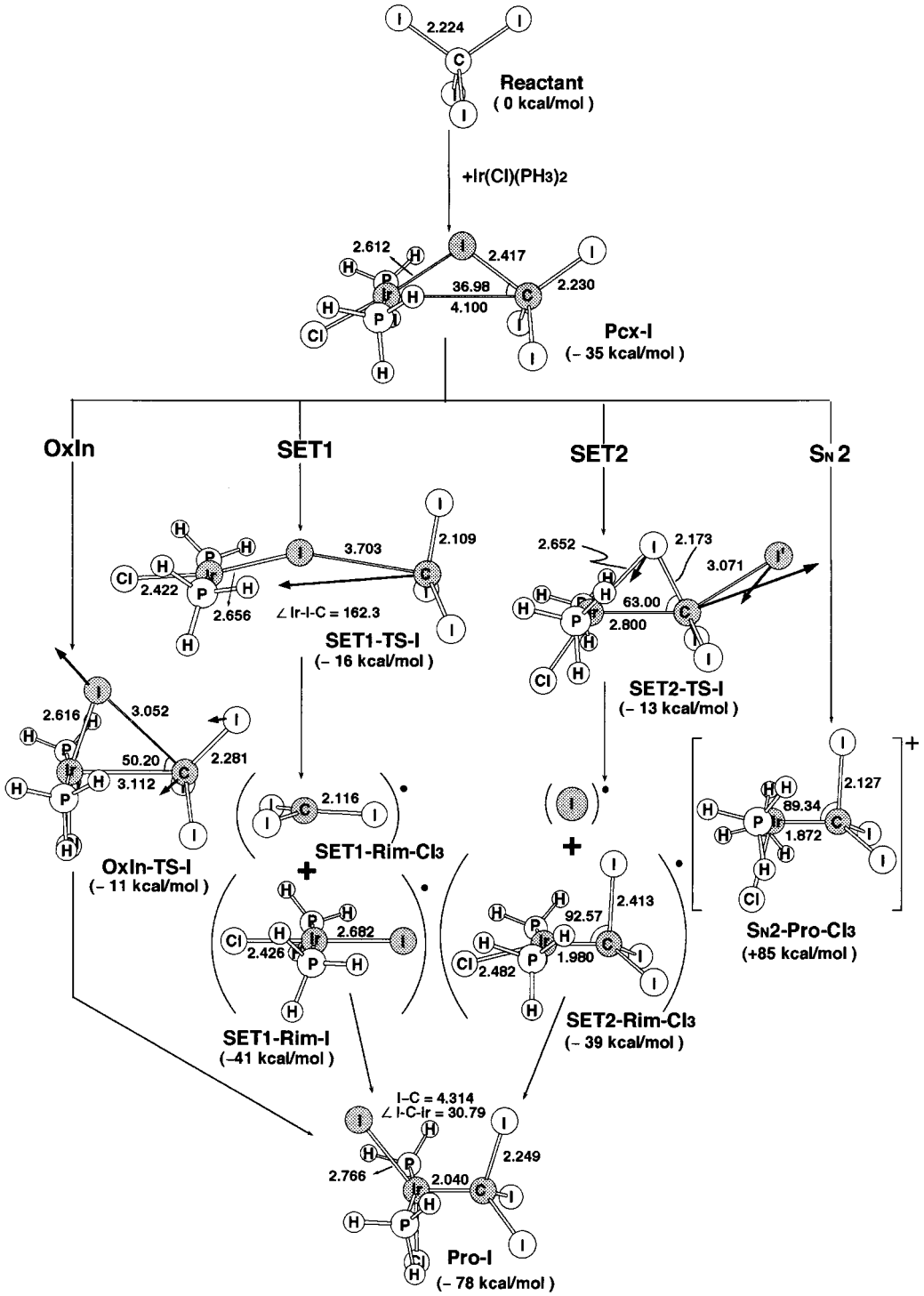

Figure 4. B3LYP/LANL2DZ optimized geometries (Å and deg) for stationary points of the *trans*-Ir(Cl)$(PH_3)_2$ + CI_4 reaction system. Values in parentheses are the relative energies at the B3LYP/LANL2DZ level. The heavy arrows indicate the main atomic motions in the transition-state eigenvector.

to carbene-like ML_n fragments.[13] Furthermore, the B3LYP/LANL2DZ results show that in **OxIn-TS-Br** and **OxIn-TS-I** the Ir−C and Ir−X (X = Br and I) distances and the Ir−C−X angle are similar in magnitude to those in the precusor complex (see Figures 3 and 4, respectively). On the other hand, in **OxIn-TS-F** and **OxIn-TS-Cl** the Ir−C and Ir−X (X = F and Cl) distances are still short, and the Ir−C−X angle resembles that of the product (see Figures 1 and 2, respectively). These features indicate that the C−Br and C−I oxidative additions reach the TS relatively early, whereas the C−F and C−Cl oxidative additions get to the TS relatively late. In other words, the heavier the tetrahalomethane system, the more reactant-like the transition-state structure. Thus, one may anticipate a smaller barrier for the CBr_4 and CI_4 insertion (vide infra).

The theoretical results depicted in Figures 1−4 reveal that all the oxidative addition products Ir(Cl)$(PH_3)_2$(X)(CX_3) adopt a distorted trigonal bipyramidal structure (T-shaped) with ligand CX_3 opposite the open site and two axial phosphines. It is intriguing to find that the Cl−Ir−X angle decreases in the order **Pro-F** (166.5°) > **Pro-Cl** (157.1°) > **Pro-Br** (153.1°) > **Pro-I** (143.2°), while the Ir−CX_3 bond distance increases in the order **Pro-F** (1.971 Å) < **Pro-Cl** (1.996 Å) < **Pro-Br** (2.005 Å) <

Table 1. Energies (kcal/mol) of Stationary Points Relative to the Reactants CX_4 + *trans*-Ir(Cl)$(PH_3)_2$ (X = F, Cl, Br, and I)[a]

system[b]	CF_4	CCl_4	CBr_4	CI_4
reactants				
CX_4 + *trans*-Ir(Cl)$(PH_3)_2$	0.0	0.0	0.0	0.0
precursor complex	−4.06[c]	−22.8[d]	−30.5[e]	−35.2[f]
OxIn				
transition states	+12.2[g]	−4.94[h]	−9.61[i]	−10.6[j]
SET1				
transition states	+33.8[k]	+1.56[l]	−6.88[m]	−16.0[n]
radical intermediates[o]				
[M]−X• + CX_3•[p]	−0.659[q]	−31.7[r]	−36.9[s]	−41.0[t]
SET2				
transition states	+42.1[u]	+0.344[v]	−5.64[w]	−12.5[x]
radical intermediates				
[M]−CX_3• + X•[p]	+15.6[y]	−24.3[z]	−35.0[aa]	−39.1[bb]
S_N2				
[M]−CX_3^+ + X^-	+148.3[cc]	+79.6[dd]	+89.9[ee]	+84.6[ff]
final products	−61.5[gg]	−71.0[hh]	−77.9[ii]	−78.2[jj]

[a] At the B3LYP/LANL2DZ level of theory; see the text. [b] See Figures 1−4 for structures. [c] Pcx-F. [d] Pcx-Cl. [e] Pcx-Br. [f] Pcx-I. [g] OxIn-TS-F. [h] OxIn-TS-Cl. [i] OxIn-TS-Br. [j] OxIn-TS-Cl. [k] SET1-TS-F. [l] SET1-TS-Cl. [m] SET1-TS-Br. [n] SET1-TS-I. [o] [M] stands for *trans*-Ir(Cl)$(PH_3)_2$. [p] The S^2 expectation values of the doublet state for the radical intermediates all show an ideal value (0.750) after annihilation, so their geometries and energetics are reliable for the present study. [q] SET1-Rim-CF_3 and SET1-Rim-F. [r] SET1-Rim-CCl_3 and SET1-Rim-Cl. [s] SET1-Rim-CBr_3 and SET1-Rim-Br. [t] SET1-Rim-CI_3 and SET1-Rim-I. [u] SET2-TS-F. [v] SET2-TS-Cl. [w] SET2-TS-Br. [x] SET2-TS-I. [y] SET2-Rim-CF_3. [z] SET2-Rim-CCl_3. [aa] SET2-Rim-CBr_3. [bb] SET2-Rim-CI_3. [cc] S_N2-Pro-CF_3. [dd] S_N2-Pro-CCl_3. [ee] S_N2-Pro-CBr_3. [ff] S_N2-Pro-CI_3. [gg] Pro-F. [hh] Pro-Cl. [ii] Pro-Br. [jj] Pro-I.

Pro-I (2.040 Å). Thus, our calculational results confirm the molecular orbital analysis of Jean and Eisenstein.[14] We suspect that such 5-coordinated products might be just local minima on the energy surface, enabling them to undergo fluxional rearrangement, of either the Berry pseudorotation or the turnstile type, to reach the global minimum. Such studies, however, are beyond the scope of the present work.

On examination of Figure 5, it is clear that, from both a kinetic and thermodynamic viewpoint, the oxidative addition reactions of CX_4 (X = Cl, Br, and I) are much more favorable than those of the CF_4 molecule. Since our model calculations demonstrate not only that the latter is thermodynamically unfavorable but also that the transition-state energy of **OxIn-TS-F** is higher than that of the reactants. On the contrary, in the former cases the energy of the transition state is below the energy of the reactants so that no net barrier to reaction exists. For instance, as shown in Table 1, the energy of the transition state relative to its corresponding reactants is (CF_4) 12.2 kcal/mol, (CCl_4) −4.94 kcal/mol, (CBr_4) −9.61 kcal/mol, and (CI_4) −10.6 kcal/mol. It is then the depth of the well for the precursor complex which determines whether the barrier lies above or below the reactant threshold. Deepening the well of the molecular complex can lower the barrier to reaction below the energy of the reactants. Therefore, the *trans*-Ir(Cl)$(PH_3)_2$ + CF_4 reaction may not have enough energy to overcome the barrier to insertion, but other *trans*-Ir(Cl)$(PH_3)_2$ + CX_4 (X = Cl, Br, and I) reactions may readily undergo oxidative addition of saturated C−X bonds in a concerted fashion.

On the other hand, if the reaction is diffusion controlled in solution or in the gas phase, then the reaction should be considered to start from the precursor complex *trans*-Ir(Cl)$(PH_3)_2\cdots CX_4$. In such cases, the ease of oxidative addition is essentially determined by the depth of the precursor complex.

(14) (a) Jean, Y.; Eisenstein, O. *Polyhedron* **1988**, *7*, 405. (b) Rachidi, I. El-I.; Eisenstein, O.; Jean, Y. *New J. Chem.* **1990**, *14*, 671. (c) Riehl, J.-F.; Jean, Y.; Eisenstein, O., Pelissier, M. *Organometallics* **1992**, *11*, 729.

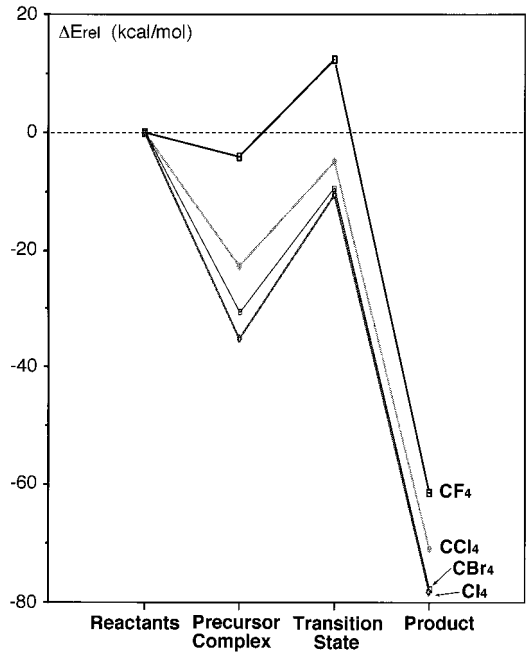

Figure 5. Reaction energy profile (kcal/mol) for the oxidative insertion (OxIn) of *trans*-Ir(Cl)$(PH_3)_2$ + X−CX_4 (X = F, Cl, Br, and I). All of the energies were calculated at the B3LYP/LANL2DZ level. See Table 1.

As demonstrated in Table 1, the energetic ordering of the addition of CX_4 to *trans*-Ir(Cl)$(PH_3)_2$ complex shows that the activation energy (relative to its corresponding precursor complex) for the process decreases in the order CF_4 (16.3 kcal/mol) < CCl_4 (17.9 kcal/mol) < CBr_4 (20.9 kcal/mol) < CI_4 (24.6 kcal/mol). Additionally, the stabilization energy of the precursor complex follows the same trend as the activation energy: CF_4 (4.06 kcal/mol) < CCl_4 (22.8 kcal/mol) < CBr_4 (30.5 kcal/mol) < CI_4 (35.2 kcal/mol). Thus, under these conditions, it will be very difficult to activate saturated C−F bonds, since the stabilization energy is so small that it cannot overcome the activation barrier. In other words, our DFT results indicate that the stronger the stabilization energy of the precursor complex, the lower the barrier height and, in turn, the easier it is to get out of the well. As there are no relevant experimental and theoretical data on such systems, the above result is a prediction.

Finally, it is obvious that all the oxidative addition reactions (left to right in Figure 5) are thermodynamically exothermic, the trend in reaction enthalpy mirroring the trend in activation energy: CF_4 (−61.5 kcal/mol) > CI_4 (−71.0 kcal/mol) > CBr_4 (−77.9 kcal/mol) > CCl_4 (−78.2 kcal/mol). Considering the reverse process (right to left in Figure 5), the B3LYP/LANL2DZ calculations suggest that the barrier to reductive elimination for the heavier halogen systems should be lower in energy than that for the lighter halogen systems. For instance, the barrier energies decrease in the order CF_4 (73.7 kcal/mol) > CCl_4 (73.3 kcal/mol) > CBr_4 (68.3 kcal/mol) > CI_4 (60.3 kcal/mol). It is therefore predicted that the greater the atomic number of halogen, the easier the reductive elimination of tetrahalomethane.

In brief summary, the carbon−halogen oxidative insertion is not only concerted (proceeding without formation of an intermediate) but also synchronous (with bond forming and breaking occurring simultaneously in the transition states of lower energy). Additionally, in the case of CCl_4, CBr_4, and CI_4 it appears that the complex potential wells are deep enough to lower the energy of the transition state for oxidative addition

of C−X (X = Cl, Br, and I) to below the energy of the reactants. We predict that, for oxidative addition of C−F, the transition-state energy is greater than the reactant energy. Thus, there is a net barrier to the C−F oxidative insertion, but no barrier to the C−X (X = Cl, Br, and I) oxidative insertion.

2. Mechanism for Radical Reactions. Next, let us consider radical mechanisms which proceed via single electron transfer (eq 2, SET), focusing on the transition states as well as the reactive intermediates. Starting from the stable precursor complex (**Pcx-F**, **Pcx-Cl**, **Pcx-Br**, and **Pcx-I** in Figures 1−4, respectively), the reaction of *trans*-Ir(Cl)$(PH_3)_2$ with CX_4 via SET can take place from two directions: the abstraction of a halogen atom X from CX_4 to produce X−[M]$^\bullet$ and $CX_3^\bullet$ intermediates (denoted SET1, shown in eq 2) and the $CX_3^\bullet$ radical transfer to [M] to lead to the formation of CX_3−[M]$^\bullet$ and X$^\bullet$ intermediates (denoted SET2), where [M] stands for *trans*-Ir(Cl)$(PH_3)_2$. Then, recombination of the radical intermediates via the metal center can result in the exothermic formation of the same insertion product. Briefly, such radical mechanisms via SET may proceed as follows: reactants → precursor complex → transition state → radical intermediates → product. The results for the transition states of the CX_4 radical reaction might perhaps be one of the most interesting results of the present study since very little is known about the barrier heights.

Several intriguing results are noteworthy.

First, considering the SET1 reaction mechanism, we have located the transition state for each CX_4 case (**SET1-TS-F**, **SET1-TS-Cl**, **SET1-TS-Br**, and **SET1-TS-I**) at the B3LYP level of theory. The optimized geometries of the four transition states can be found in Figures 1−4, respectively, along with the imaginary frequency eigenvector. One can observe that the main components of the transition vector correspond to the motion of the halogen atom (X) between the iridium and the carbon atoms, whose eigenvalue gives an imaginary frequency of 1044i (**SET1-TS-F**), 314i (**SET1-TS-Cl**), 131i (**SET1-TS-Br**), and 113i (**SET1-TS-I**) cm^{-1}. The transition states involve the approach of *trans*-Ir(Cl)$(PH_3)_2$ along the X−C axis of the CX_4 molecule. The three atoms (Ir, X, and C) involved in the bond-breaking and bond-forming processes are not collinear along the X−C axis as shown in Figures 1−4. The iridium atom of the *trans*-Ir(Cl)$(PH_3)_2$ complex makes an angle, with respect to the X−C bond, of 156°, 164°, 178°, and 162° for CF_4, CCl_4, CBr_4, and CI_4, respectively. Interestingly, the approach of the *trans*-Ir(Cl)$(PH_3)_2$ along the X−C axis is more bent in the CF_4 case than in the CCl_4, CBr_4, and CI_4 cases. The breaking X−C bond length is generally increased, while the forming Ir−X bond length becomes smaller. For reactions of *trans*-Ir(Cl)$(PH_3)_2$ with CF_4, CCl_4, CBr_4, and CI_4, the breaking X−C bond lengths are 3.578 Å (F), 4.095 Å (Cl), 3.793 Å (Br), and 3.703 Å (I), respectively, while the forming Ir−X bond lengths are 0.019 Å (F), 0.019 Å (Cl), 0.023 Å (Br), and 0.026 Å (I) shorter than that in *trans*-Ir(Cl)$(PH_3)_2$−X$^\bullet$ intermediate. This suggests that the delocalization of the unpaired electron takes place later along the reaction coordinate. Thus, the changes in the X−C and Ir−X bond lengths in the transition structure are more reactant-like for X = Br and I, in accordance with the large exothermicity of the abstraction process. As demonstrated below, this is consistent with the Hammond postulate[15] which associates an earlier transition state with a smaller barrier and a more exothermic reaction.

Second, optimized geometries for *trans*-Ir(Cl)$(PH_3)_2$−X$^\bullet$ (**SET1-Rim-F**, **SET1-Rim-Cl**, **SET1-Rim-Br**, and **SET1-Rim-I**) radicals are also given in Figures 1−4, respectively. Basically, these radicals adopt a ML_4 square-planar geometry, in which chlorine is trans to the incoming halogen atom X. The B3LYP calculations show that in these radicals the trans Ir−Cl bond distance is somewhat larger in the CBr_4 and CCI_4 cases than that in the CF_4 and CCl_4 cases (about 0.012 Å longer). We attribute the long trans Ir−Cl distance in the former two radicals to the stronger trans-destabilizing effect of Br and I compared to F and Cl.[16] On the other hand, as demonstrated in Figures 1−4 (see **SET1-Rim-CF_3**, **SET1-Rim-CCl_3**, **SET1-Rim-CBr_3**, and **SET1-Rim-CI_3**, respectively) the flap angle at carbon of the CX_3 radical decreases uniformly as halogen X is changed from F (55.2°) to Cl (40.6°) to Br (34.3°) and then to I (12.3°). That is to say, the geometry of CX_3 radical becomes strongly pyramidal when halogen X becomes more electronegative.[17] Furthermore, it is interesting to note that, when CX_3 is the leaving group in the SET1 mechanism, the coordination at carbon is strongly pyramidal in **SET1-TS-F** and **SET1-TS-Cl**. In contrast, **SET1-TS-Br** and **SET1-TS-I** show a more planar, less pyramidal coordination geometry at carbon. In other words, the pyramidalization at the CX_3 moiety decreases rapidly from F down to I. This is consistent with the structure of the CX_3 radical as discussed above.

Third, considering the SET2 mechanism, a search for the transition state did show that the energy profile for this reaction exhibits a maximum. The transition states located for the CX_3 (X = F, Cl, Br, and I) abstractions are presented in Figures 1−4, respectively. Those transition structures are characterized by one imaginary frequency of 421i, 368i, 243i, and 509i cm^{-1} for **SET2-TS-F**,[12] **SET2-TS-Cl**, **SET2-TS-Br**, and **SET2-TS-I**, respectively. The normal coordinate corresponding to the imaginary frequency is primarily the motion of the halogen atom (X′) separating from the carbon atom of CX_3. Therefore, the reaction coordinate is fundamentally an asymmetric stretch at the conventional transition state. Further, as was the case for halogen atom abstraction (SET1), the leaving halogen atom X′ does not lie on the Ir−C axis. Additionally, It was found that, in the transition structure for the CX_3 abstraction process, the CF_3 moiety has a strongly pyramidal carbon center, while the CI_3 moiety has a nearly planar coordination around carbon. Namely, the lighter the halogen atom, the stronger the pyramidalization at the CX_3 moiety. Again, this is consistent with the structure of the CX_3 radical as discussed previously in the SET1 case. Moreover, the transition structures show that the newly formed Ir−C bond length is 2.006 Å (**SET2-TS-F**), 2.050 Å (**SET2-TS-Cl**), 2.673 Å (**SET2-TS-Br**), and 2.800 Å (**SET2-TS-I**), compared to that in the radical intermediate of 2.013 Å (**SET2-Rim-F**), 1.999 Å (**SET2-Rim-Cl**), 1.986 Å (**SET2-Rim-Br**), and 1.980 Å (**SET2-Rim-I**), respectively. Also, in the case of CF_4 and CCl_4, the Ir−C−F (79.01°) and Ir−C−Cl (75.80°) angles are significantly longer than in the case of CBr_4 (62.55°) and CI_4 (63.00°). Similarly, the C−F and C−Cl bond lengths are shorter (i.e., 1.558 Å in **SET2-TS-F** and 2.087 Å in **SET2-TS-Cl**), which are close to those in the radical intermediates, 1.445 Å (**SET2-Rim-F**) and 1.962 Å (**SET2-Rim-Cl**), respectively. Taken together these features indicate that the transition structures for CF_4 and CCl_4 take on more productlike character than those for CBr_4 and CI_4. This is in accord with the greater exothermicity of the *trans*-Ir(Cl)$(PH_3)_2$ + CX_4 (X = Br and I) reaction than that of the *trans*-Ir(Cl)$(PH_3)_2$ + CF_4 reaction (see below).

(15) Hammond, G. S. *J. Am. Chem. Soc.* **1954**, *77*, 334.

(16) (a) Cotton, F. A.; Wilkinson, G. *Advanced Inorganic Chemistry*, 5th ed.; Wiley: New York, 1988; p 1299. (b) Burdett, J. K.; Albright, T. A. *Inorg. Chem.* **1979**, *18*, 2112.

(17) Gimarc, B. M. *Molecular Structure and Bonding*; Academic Press: New York, 1979; p 169.

Fourth, the results obtained for the CX_3 abstraction process are an interesting example where the knowledge of the structure of the transition state and the transition vector is not sufficient to assess the type of reaction, i.e., whether the SET2 path leads to abstraction or S_N2 reaction. Only a study of the instrinic reaction coordinate (IRC) can provide this information. We therefore chose the *trans*-Ir(Cl)$(PH_3)_2$ + CF_4 reaction as a model system to study its IRC for reaction of type SET2. The results of these computations (in particular the behavior of the most significant geometrical parameters along the IRC starting from the saddle point toward the product) are shown in Figure 6. For the abstraction of CF_3 we follow the IRC until the C−F bond is completely broken (2.842 Å). As the reaction proceeds, the Ir−C distance decreases from a value of 2.006 Å in **SET2-TS-F** to a value of 1.956 Å at the fourth point on the IRC. The Ir−C distance subsequently increases, albeit by a small amount (1.970 and 1.976 Å at points 6 and 7), when the two newly formed radical fragments (*trans*-Ir(Cl)$(PH_3)_2$−$CF_3^\bullet$ and $F^\bullet$) move apart. The phenomenon can be simply understood as follows. When the C−F bond begins to break, there is a tendency for the unpaired electron to delocalize across the orbitals of the newly formed Ir−C bond, thereby reducing its bonding character. This, in turn, will result in an increase in the Ir−C bond distance. Alternatively, for an S_N2 pathway, the Ir−C bond formation is preceded by a monotonic decrease in the Ir−C bond distance. Consequently, this IRC evidence strongly indicates that the transiton state **SET2-TS-F** we found in this study corresponds to the abstraction of $CF_3^\bullet$. Likewise, identical conclusions can be drawn for SET2 reaction pathways involving CCl_4 (**SET2-TS-Cl**), CBr_4 (**SET2-TS-Br**), and CI_4 (**SET2-TS-I**), as shown in Figures 2−4, respectively.

Fifth, the equilibrium geometries for *trans*-Ir(Cl)$(PH_3)_2$−$CX_3^\bullet$ (**SET2-Rim-CF_3**, **SET2-Rim-CCl_3**, **SET2-Rim-CBr_3**, and **SET2-Rim-CI_3**) radicals are presented in Figures 1−4, respectively. All of these radicals adopt a ML_4 square-planar geometry, in which chlorine is trans to the incoming CX_3 group. The DFT calculations suggest that the trans Ir−Cl bond distance increases in the order **SET2-Rim-CF_3** (2.463 Å) < **SET2-Rim-CCl_3** (2.468 Å) < **SET2-Rim-CBr_3** (2.472 Å) < **SET2-Rim-CI_3** (2.482 Å). Again, this result confirms the conventional finding that the substitution of a more electronegative ligand (such as CF_3 and CCl_3) will strengthen the trans Ir−Cl bond.[16]

Sixth, in the SET1 approach, examination of the energy values collected in Table 1 shows that at the B3LYP/LANL2DZ level the Br and I abstractions are favored. A schematic diagram of the *trans*-Ir(Cl)$(PH_3)_2$ + CX_4 (X = F, Cl, Br, and I) potential surface via SET1 is displayed in Figure 7. The present calculations predict that the energies of **SET1-TS-F** and **SET1-TS-Cl** are above those of the reactants by 33.8 and 1.56 kcal/mol and the activation energies for the overall reaction are 37.9 and 24.4 kcal/mol, respectively. In contrast, the DFT results suggest that the energies of **SET1-TS-Br** and **SET1-TS-I** are below those of reactants, so that no net barrier to reaction exists. Additionally, the activation energy from the corresponding precursor complex for Br abstraction is 23.6 kcal/mol, and that for I abstraction is 19.2 kcal/mol. This is consistent with the observations shown earlier, in which for the case of CBr_4 and CI_4 the saddle point lies much closer to reactants than products. Moreover, for a given metal, it is generally found that (a) the overall SET1 reaction for each CX_4 case is exothermic and the exothermicity follows the same trend as in the oxidative insertion described earlier and (b) the overall barrier heights are determined to be in the order CF_4 > CCl_4 > CBr_4 > CI_4. In any event, the smaller barrier for the latter two cases relative to the former two cases reflects the greater ease of abstracting a halogen from CBr_4 and CI_4 over abstraction from CF_4 and CCl_4. Namely, the heavier the halogen atom (X), the more facile the abstraction of a halogen from CX_4. Finally, it is worth pointing out that the reverse of reaction SET1 is the dissociation of the Ir(Cl)$(PH_3)_2$(X)(CX_3) product to *trans*-Ir(Cl)$(PH_3)_2$−$X^\bullet$ and $CX_3^\bullet$. Accordingly, from Table 1 one may easily, albeit roughly, estimate the bonding energy of the Ir−CX_3 bond, which decreases in the order Ir−CF_3 (95.4 kcal/mol) > Ir−CCl_3 (79.8

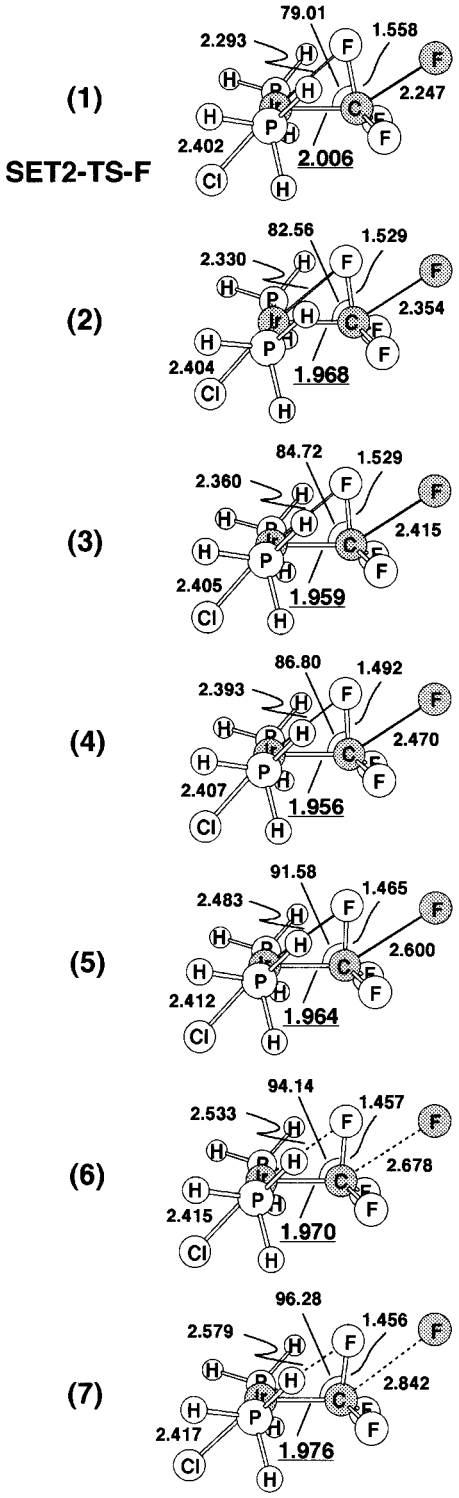

Figure 6. Structures determined along the intrinsic reaction coordinate (IRC) for the CF_3 abstraction by *trans*-Ir(Cl)$(PH_3)_2$ (bond lengths are in angstroms and angles in degrees). See the text.

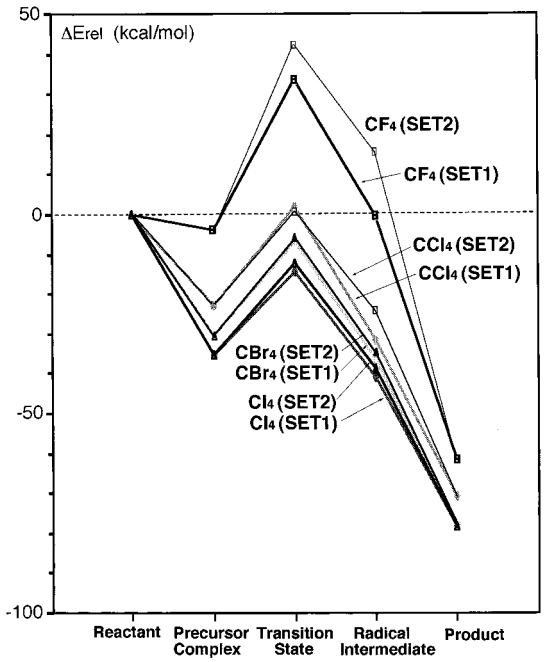

Figure 7. Reaction energy profile (kcal/mol) for radical pathways (SET1 and SET2) of *trans*-Ir(Cl)$(PH_3)_2$ + X−CX_4. All of the energies were calculated at the B3LYP/LANL2DZ level. See the text and Table 1.

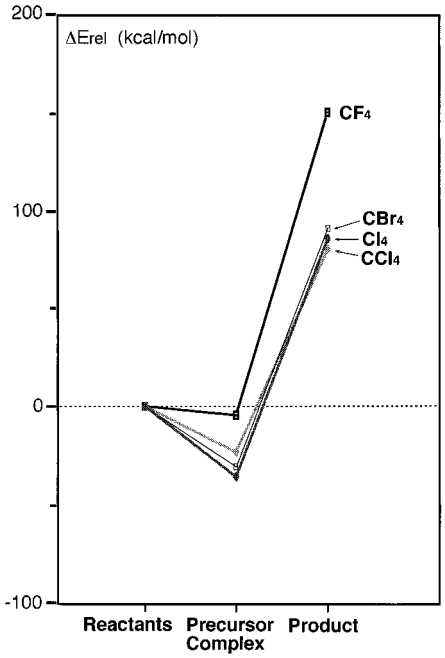

Figure 8. Reaction energy profile (kcal/mol) for the nucleophilic substitution (S_N2) of *trans*-Ir(Cl)$(PH_3)_2$ + X−CX_4 (X = F, Cl, Br, and I). All of the energies were calculated at the B3LYP/LANL2DZ level. See the text and Table 1.

kcal/mol) > Ir−Br_3 (71.0 kcal/mol) > Ir−CI_3 (55.0 kcal/mol).

The energetics for reactions of the type *trans*-Ir(Cl)$(PH_3)_2$ + CX_4 (X = F, Cl, Br, and I) via SET2 are also summarized in Table 1 and in Figure 7. The most dramatic change occurs in the position of radical intermediate **SET2-Rim-CF_3** on the reaction paths, whose energy is apparently higher than the energy of the corresponding reactants by 15.6 kcal/mol, whereas the energies of other radicals are lower than those of the reactants. By analogy with the SET1 reaction pathway, only the energies of **SET2-TS-F** and **SET2-TS-Cl** were calculated to be 42.1 and 0.344 kcal/mol, respectively, higher than those of the reactants. In addition, the overall barrier with respect to the corresponding precursor complex for CX_3 abstraction was estimated to be 46.1 (**SET2-TS-F**), 23.2 (**SET2-TS-Cl**), 24.8 (**SET2-TS-Br**),and 22.7 (**SET2-TS-I**) kcal/mol. Note that the forward barrier for abstracting a CX_3 group from CX_4 (X = Cl, Br, and I) is half the size of that for the CF_4 case. Consequently, our theoretical results reaffirm the Hammond postulate as discussed earlier and predict that the process for abstracting a CBr_3 or CI_3 group should be more facile than that for abstracting a CF_3 or CCl_3 group. From another point of view, this strongly implies that the leaving group tendency increases in the order F < Cl < Br < I. Moreover, this result reinforces the trend expressed earlier that the bonding energy of C−X decreases in the order C−F (116 kcal/mol) > C−Cl (78.2 kcal/mol) > C−Br (68 kcal/mol) > C−I (51 kcal/mol).[5] On the other hand, from the adduct Ir(Cl)$(PH_3)_2$(X)(CX_3) energies obtained in Table 1, the Ir−F, Ir−Cl, Ir−Br, and Ir−I single-bond energies (the reverse of reaction SET2) were calculated to be 104, 78.6, 75.6, and 58.5 kcal/mol, respectively, i.e., again following the same trend along the series X = F, Cl, Br, and I.

Comparison of the CX_4 abstraction pathways for X = F, Cl, Br, and I reveals interesting similarities and differences. As for the similarities, two similar abstraction pathways (SET1 and SET2) exist for each CX_4 case even though the energetics are different. Furthermore, the *trans*-Ir(Cl)$(PH_3)_2$ + CF_4 abstraction reaction is found to have the highest barrier with identical exothermicities via both routes. Additionally, since the transition states for SET1 and for SET2 are predicted to have similar energy for the CX_4 (X = Cl, Br, and I) systems, either approach should be competitive. While the similarities between the two pathways for each CX_4 system are remarkable, the differences between them are more significant. The most noted difference is in the CF_4 abstraction reaction. The computed B3LYP/LANL2DZ barriers are 33.8 kcal/mol for F abstraction (SET1) and 42.1 kcal/mol for CF_3 abstraction (SET2); thus, the former is energetically favored.

In short, the present calculations suggest the following about the radical mechanism for the *trans*-Ir(Cl)$(PH_3)_2$ + CX_4 reaction: *(1) Carbon−halogen activation may proceed via a two-step abstraction−recombination path (formation of the two radicals collapsing in a subsequent step to the final product). (2) Fluorine abstraction is predicted to be faster than the abstraction a CF_3 group. In contrast, for CCl_4, CBr_4, and CI_4 systems, abstraction of halogen (X) and CX_3 fragments are found to be kinetically competitive. (3) The reaction rates for trans-Ir(Cl)$(PH_3)_2$ + CF_4 and CCl_4 via both SET1 and SET2 routes are expected to be significantly slower than those for CBr_4 and CI_4.*

3. Mechanism for Substitution Reactions. Finally, we turn our attention to the nucleophilic substitution reaction (S_N2). Traditionally, the backside S_N2 substitution plays a dominant role in the organic reaction systems.[18] We have extended this concept to the organometallic system studied in this work. The calculated reaction profiles for *trans*-Ir(Cl)$(PH_3)_2$ insertion into CX_4 (X = F, Cl, Br, and I) via an S_N2 pathway are collected in Figure 8.

Starting from the stable precursor complex, attempts were made to locate the transition states for the S_N2 pathways, but no transition state could be found in each CX_4 case. This is easily explained by the molecular orbital analysis. As already

(18) (a) March, J. *Advanced Organic Chemistry*; Wiley-Interscience: New York, 1992. (b) Deng, L.; Branchadell, V.; Ziegler, T. *J. Am. Chem. Soc.* **1994**, *116*, 10645.

shown in **1**, a *trans*-Ir(Cl)$(PH_3)_2$ fragment has a dπ-type HOMO, which will interact with the backside of the σ orbital of CX_4. From **2** we see that this interaction is, however, very poor, since

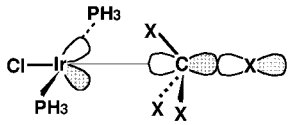

2

the σ orbital approahes on a nodal surface of the HOMO lobe, resulting in a cancellation of overlap. Thus, it would be unlikely to find the transition state along the backside reaction coordinate.

Alternatively, the backside S_N2 substitution may proceed through the "straight" S_N2 path,[6] i.e., via attack of Ir on carbon and expulsion of the X^- leaving group to produce the products *trans*-Ir(Cl)$(PH_3)_2(CX_3)^+ + X^-$. It is apparent from Figure 8 and Table 1 that the energies of the products *trans*-Ir(Cl)$(PH_3)_2$-$(CX_3)^+ + X^-$ are much higher than those of the corresponding reactants by 148, 79.6, 89.9, and 84.6 kcal/mol for **Pro-SN2-F**, **Pro-SN2-Cl**, **Pro-SN2-Br**, and **Pro-SN2-I**, respectively. The reason for such high endothermicities is due to the development of a charge separation in the products. As a result of the high endothermicity of these S_N2 reactions, they do not constitute a competitive pathway for the formation of Ir(Cl)$(PH_3)_2$(X)(CX_3) in the gas phase.[19]

4. Overview of C−X Activation Reactions. From our survey of the mechanisms of the *trans*-Ir(Cl)$(PH_3)_2 + CX_4$ reactions, we can obtain the following conclusions: *(a) Considering both the activation barrier and exothermicity based on the model calculations presented here, we conclude that for the oxidative addition of trans-Ir(Cl)$(PH_3)_2$ by insertion into $X-CX_3$, the order of reactivity is I > Br > Cl ≫ F, whether diffusion control operates. This may be a reflection of the carbon−halogen bond strengths. (b) The trans-Ir(Cl)$(PH_3)_2$ fragment insertion into C−F and C−Cl bonds (OxIn) is anticipated to be in favor of oxidative additions. On the contrary, the SET mechanism proceeding via either a halogen or a CX_3 abstraction by trans-Ir(Cl)$(PH_3)_2$ and recombination of the intermediates (eq 2) has a barrier comparable to that for oxidative insertions in the CBr_4 and CI_4 systems. In other words, the ease of oxidative insertion increases with increasing halogen electronegativity. OxIn and SET pathways constitute competitive reaction pathways for the heavier halogens, particularly iodine. (c) In the competition of the S_N2 path with OxIn and SET processes, the former has the highest energy requirement and therefore is the least energetically favorable path in the gas phase.*

IV. Configuration Mixing Model

All these computational results can be rationalized on the basis of a simple valence bond (VB) model based upon reactant and product spin recoupling, which is often described as the configuration mixing (CM) model.[20,21] In this approach the total energy profile is decomposed into two components, one associated with the reactant spin coupling and the other with the product spin coupling. These two component curves are

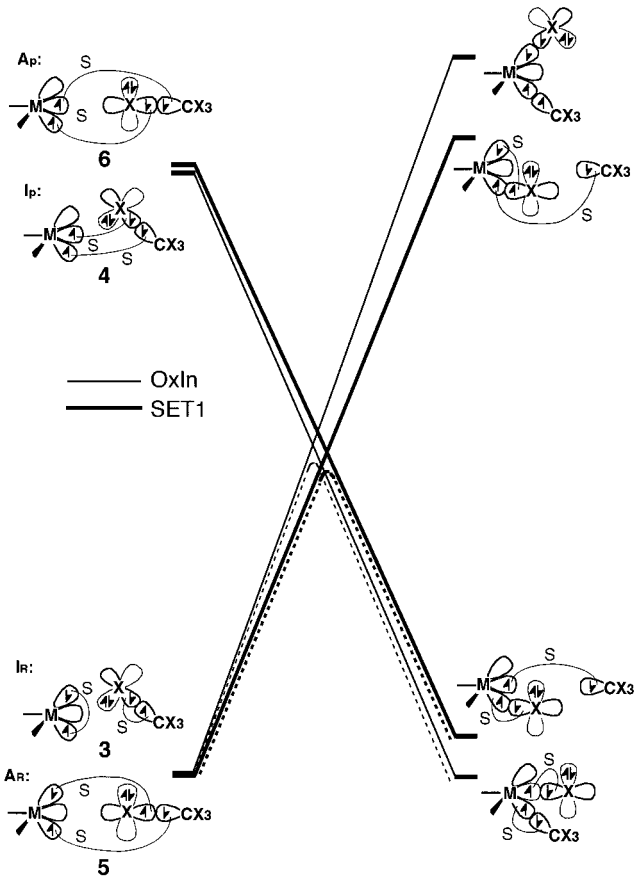

Figure 9. Qualitative state correlation diagram for the oxidative insertion (OxIn) and the radical pathway (SET1) showing the formation of a state curve by mixing two configurations: the reactant configuration (**3**, I_R; **5**, A_R) and the product configuration (**4**, A_P; **6**, I_P). It is apparent that both the activation energy ($\Delta E^{\ddagger}$) and reaction enthalpy (ΔH) are proportional to ΔE_{st} ($+ E_{triplet} - E_{singlet}$ for 14-electron ML_3) and $\Delta E_{\sigma\sigma^*}$ ($= E_{triplet} - E_{singlet}$ for CX_4). See the text.

denoted as *reactant configuration* and *product configuration*, respectively. It follows that, on going from reactants to products, the reactant configuration curve is repulsive and the product configuration curve attractive (see below). The crossing of the two curves detects the transition state and the energy barrier.

In Figure 9, we represent the qualitative behavior of the two configurations for T-shaped ML_3 oxidative addition to a C−X bond. For convenience, we only consider two reactions: oxidative insertion (OxIn, eq 1) and halogen abstraction (SET1 in eq 2). We use I_R and I_P to denote the insertion reactant−product spin coupling and A_R and A_P to denote the abstraction reactant−product spin coupling. I_R describes a situation where the two electrons on the ML_3 fragment are spin-paired to form the lone pair, while the two electrons on the CX_4 moiety are spin-paired to form a C−X σ bond as illustrated in **3**. I_P

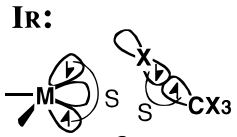

3

corresponds to a situation where the electron pairs are coupled to allow both M−X and M−CX_3 bond formation and simultaneous C−X bond breaking. See **4**. To obtain this configuration from the reactant configuration I_R **(3)**, each of the two original electron pairs needs to be uncoupled, requiring the excitation

(19) Presumably, solvent effects might tend to favor the straight S_N2 substitution due to the charge separation in the products. Though we have not carried out such a calculation in this work, S_N2 cannot be generally excluded as a pathway in the solvent phase. We thank one reviewer for bringing this phenomenon to our attention.

(20) (a) Shaik, S.; Schlegel, H. B.; Wolfe, S. *Theoretical Aspects of Physical Organic Chemistry*; John Wiley & Sons Inc.: New York, 1992. (b) Pross, A. *Theoretical and Physical principles of Organic Reactivity*; John Wiley & Sons Inc.: New York, 1995.

(21) Su, M.-D. *Inorg. Chem.* **1995**, *34*, 3829.

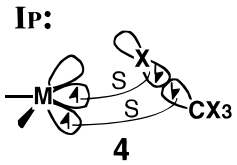

4

of the electron pairs from the singlet state to the triplet state. Thus, I_P describes an overall singlet configuration, despite the fact that it contains two local triplets. A_R describes the singlet spin-coupled CX_3 pσ orbital and the ML_3 dπ orbital (HOMO, **1b**), the halogen pσ orbital and the ML_3 HOMO being singlet spin-coupled as shown in **5**. On the other hand, A_P (**6**) describes

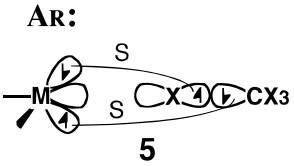

5

the singlet spin-coupled ML_3 HOMO and halogen pσ orbitals, the CX_3 pσ orbital and the ML_3 LUMO being singlet spin-coupled. At infinite separation (left side in Figure 9), the states

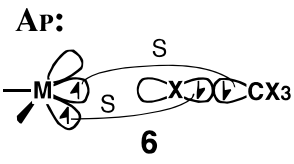

6

corresponding to spin coupling A_R and I_R are at the same energy level since both contain the singlet ML_3 fragment and CX_4 molecule. In contrast, on the product side (right bottom side in the diagram of Figure 9) the energy of the insertion product is lower than that of the abstraction product as given in Table 1. As mentioned above, it is the avoided crossing of the reactant and product configurations (I_R and I_P; A_R and A_P) that leads to the simplest description of the ground-state energy profiles for oxidative addition reactions of 14-electron T-shaped ML_3 complexes. Bearing this CM model (Figure 9) in mind, we shall explain the origin of the observed trends as shown previously in the following discussion.

(a) Why Does the Ease of C−X Oxidative Addition Increase in the Order C−F < C−Cl < C−Br < C−I? The reason for this can be traced to the singlet−triplet energy gap of CX_4. As shown in Figure 9, it is apparent that the barrier height ($\Delta E^{\ddagger}$) as well as the reaction enthalpy (ΔH) may be expressed in terms of the initial energy gap between the reactant and product configurations. Consider the reactant and product configurations for the insertion reaction, i.e., I_R (**3**) and I_P (**4**), respectively. The CM model shows that the existence of the barrier is due to the combined effect of two factors: the singlet−triplet energy gap of T-shaped ML_3 ($\Delta E_{st} = E_{triplet} - E_{singlet}$ for 14-electron ML_3) and the σ(C−X) → σ*(C−X) triplet excitation energy of CX_4 ($\Delta E_{\sigma\sigma^*} = E_{triplet} - E_{singlet}$ for CX_4). Accordingly, supposing ΔE_{st} is a constant, a smaller value of $\Delta E_{\sigma\sigma^*}$ would lead to (1) reduction of the reaction barrier since the intended crossing of IR and IP is lower in energy and (2) a larger exothermicity since the energy of the product is now lower than that of the reactant.[20,21]

Furthermore, a diagram that illustrates qualitatively the relative σ and σ* energy levels for the C−X bonds is shown in Figure 10.[22] From Figure 10, it is obvious that σ energy levels

Figure 10. Schematic representation of the relative energy levels for σ and σ* levels for C−F, C−Cl, C−Br, and C−I bonds. See ref 22.

increase from F to I (i.e., σ(C−F) < σ(C−Cl) < σ(C−Br) < σ(C−I)), whereas σ* energy levels decrease from F to I (i.e., σ*(C−F) > σ*(C−Cl) > σ*(C−Br) > σ*(C−I)). This strongly implies that the σ(C−X) → σ*(C−X) triplet excitation energy of CX_4 becomes smaller as one proceeds along the series from F to I. Indeed, our DFT calculations confirm this prediction and suggest a decreasing trend in $\Delta E_{\sigma\sigma^*}$ for CF_4 (266 kcal/mol) > CCl_4 (110 kcal/mol) > CBr_4 (73 kcal/mol) > CI_4 (47 kcal/mol).[23] From Table 1, it is readily seen that this result is in accordance with the trend in activation energy and enthalpy ($\Delta E^{\ddagger}$, ΔH) for *trans*-Ir(Cl)$(PH_3)_2$ insertion which are (12.2, −61.5), (−4.94, −71.0), (−9.61, −77.9), and (−10.6, −78.2) kcal/mol,[24] respectively. Note that the order of $\Delta E_{\sigma\sigma^*}$ is just the C−X bond strength order.[5] Consequently, our theoretical findings are in good agreement with the CM model.

(b) Why Does the Ease of Halogen Abstraction from CX_4 Increase in the Order $F^{\bullet}$ < $Cl^{\bullet}$ < $Br^{\bullet}$ < $I^{\bullet}$? If we refer to Figure 9, it can be seen that the transition state is associated with the crossing of A_R and A_P. Thus, by analogy with the insertion case discussed above, the driving force for such abstraction reactions may be traced to $\Delta E_{\sigma\sigma^*}$. Namely, the smaller the $\Delta E_{\sigma\sigma^*}$ of CX_4, the lower the barrier height and, in turn, the faster the abstraction reaction, the larger the exothermicity.[15] As a result, on comparison of the $\Delta E_{\sigma\sigma^*}$ of CX_4 with the abstraction barriers as given in Table 1, it is easy to see that the intrinsic reactivity order $F^{\bullet}$ < $Cl^{\bullet}$ < $Br^{\bullet}$ < $I^{\bullet}$ is the reverse of the order of $\Delta E_{\sigma\sigma^*}$. Likewise, the same explanation can also be applied to the CX_3 abstraction, which follows the same order as the halogen abstraction as shown in Table 1: $CF_3^{\bullet}$ < $CCl_3^{\bullet}$ < $CBr_3^{\bullet}$ < $CI_3^{\bullet}$.

(c) Why Is the CF_4 (or CCl_4) Molecule Relatively in Favor of Insertion but Unreactive to Abstraction, Whereas the CI_4 (or CBr_4) Molecule Is Reactive to Both? According to the CM model discussed previously, it is clear that the reactivity order for both insertion and abstraction is governed by the magnitude of $\Delta E_{\sigma\sigma^*}$ of CX_4. Besides this, the nonbonded

(22) Reference 20b, p 51.

(23) $\Delta E_{\sigma\sigma^*}$ can be evaluated to a good approximation from the energies of the vertical σ(C−X) → σ*(C−X) triplet excitation in CX_4 (X = F, Cl, Br, and I).

(24) It has to be emphasized that calculated DFT barrier heights are often, if anything, too low; see: *Chemical Applications of Density Functional Theory*; Laird, A., Ross, R. B., Zeigler, T., Eds.; American Chemical Society: Washington, DC, 1996. Thus, those barrier numbers might be underestimated by several kilocalories per mole. It is believed that using the more sophisticated theory with larger basis sets should be essential. Nevertheless, the energies obtained at the B3LYP/LANL2DZ level can, at least, provide the reliably qualitative conclusions.

repulsive interactions also play a significant role in the C−X oxidative additions. On one hand, in comparison of I_R (**3**) with A_R (**5**), one may easily see that the latter should be more strongly repulsive than the former (see Figure 9). The reason for this is because the lone pairs of X are pointing toward the empty LUMO σ orbital of the ML_3 fragment in the former case, whereas there exist repulsive interactions between the lone pairs of X and the HOMO of the ML_3 complex in the latter case.[25] Consequently, A_R must rise more steeply than I_R along the reaction coordinate and yield a higher barrier as a result of crossing with A_P and I_P, respectively. This would result is a smaller barrier height for insertion than for abstraction. This is what we observed in the CF_4 and CCl_4 systems.

On the other hand, in the case of attack at a halogen atom (see A_P as in **6**), at the point where the new M−X bond is almost formed one may have two new radical fragments, X−[M]$^\bullet$ and $CX_3^\bullet$, where the singlet spin coupling of the CX_3 pσ orbital to the ML_3 LUMO has taken place. In contrast, in the case of insertion (see I_P as in **4**), the formation of a second bond involves singlet spin coupling of the CX_3 pσ orbital to the ML_3 HOMO. Accordingly, the position of X (located in the region between those two radical fragments) causes the appearance of repulsive interactions due to the presence of the X lone pairs, and the reactants cannot approach closely enough to allow the singlet spin coupling of the CX_3 pσ orbital to the ML_3 HOMO. This would result in the fact that A_P decreases more rapidly than I_P as the reactants approach each other and yields a lower barrier as a result of their crossing with A_R and I_R, respectively. In particular, such lone pair repulsions will be magnified in the CI_4 and CBr_4 cases, since I and Br possess more diffuse p orbitals than F and Cl. As a result, in the C−I and C−Br oxidative additions, barrier heights for both insertion and abstraction might be nearly equal, and thus the two pathways may occur in parallel. This is consistent with the observed relative reactivities of these compounds.

V. Conclusion

In this paper three different possible mechanisms for the oxidative addition of 14-electron *trans*-Ir(Cl)$(PH_3)_2$ complex to the saturated carbon−halogen bonds have been systematically studied. The transition states and associated energy barriers for the insertion of *trans*-Ir(Cl)$(PH_3)_2$ into the C−X bonds of CX_4 have been considered. Halogen atom and CX_3 abstraction reactions, in addition to backside S_N2 substitution reactions, have also been determined at the same level of theory. It has to be pointed out that the present calculations provide the first theoretical estimation of the activation energy for these processes and qualitative evidence for the feasibility of such elementary reactions. Our calculations based on the B3LYP/LANL2DZ level of theory suggest that insertions into either a saturated C−F bond or a saturated C−Cl bond generally occur with smaller barriers than the corresponding abstractions. It is therefore reasonable to conclude that the mechanism depicted in eq 1 (OxIn) should be the most likely pathway for the CF_4 and CCl_4 systems. On the contrary, kinetically, both insertions and abstractions are found to be competitive for the CI_4 and CBr_4 systems. In principle, considering both the activation barrier and exothermicity on the basis of the model calculations presented here, it is therefore concluded that for the oxidative addition reaction of X−CX_3 to 14-electron T-shaped ML_3 complex, the order of reactivity is Cl > Br > I ≫ F, whether diffusion control operates. Furthermore, in the case of the backside S_N2 substitution, because of the significantly high barrier, this reaction is unlikely to occur at room temperature for any of the CX_4 systems in the gas phase.[19] Unfortunately, as we have mentioned earlier, because of a lack of experimental and theoretical data on such C−X bond activations, our conclusions above may be considered as predictions for future investigations.

Aside from the importance of the investigation of those possible reaction mechanisms, it is also interesting to compare various transition states in the present work. The interpretation of the computational results is less obvious for the two transition states found for the singlet reaction. For instance, in the CF_4 case analysis of the transition structures and the corresponding transition vectors did not provide enough information to determine what type of reaction (i.e., a CX_3 fragment abstraction or an S_N2 substitution) was occurring. This difficulty has been solved by computing the IRC. The IRC results have highlighted the usefulness of this technique in elucidating reaction mechanisms and have clearly demonstrated what kind of reactions are involved. Also, we have demonstrated that the computational results can be rationalized using a simple CM model. This model showed that the lower barrier of the C−X oxidative additions is a consequence of (a) the energy difference between the reactant and product configurations and (b) the halogen lone pair repulsions. Nevertheless, a word of caution has to be stressed here. The preference for F insertion over F abstraction does not necessarily hold for carbene-like ML_n metal complexes. For instance, the 14-electron ML_2 fragment may prefer to adopt the F abstraction rather than the F insertion pathway due to the strong repulsions between the F lone pairs and the ML_2 frontier orbitals.[26]

Although generalization of the results presented here might be questioned by the limitations of the applied methodology, we think that the level of interest in this subject and the important implications suggested by these results make further research in this area a priority.

We encourage experimentalists to carry out further experiments to confirm our predictions.

Appendix

All geometries were fully optimized without imposing any symmetry constraints. For our DFT calculations, we used the hybrid gradient-corrected exchange functional proposed by Becke,[27a,b] combined with the gradient-corrected correlation functional of Lee, Yang, and Parr.[27c] This functional is commonly known as B3LYP, and has been shown to be quite reliable for geometries.[28]

Effective core potentials (ECPs) were used to represent the 60 innermost electrons of the iridium (up to the 4f shell) atom.[29] Likewise, for phosphor, chlorine, bromine, and iodine we used the Hay and Wadt relativistic effective core potential (ECP).[30] For these atoms, the basis set was that associated with the

(25) Further supporting evidence comes from the fact that in geometrical structures of the OxIn transition states the lone pairs of electrons on the halogen atom interact with the empty s/p/d hybridized orbital (i.e., the LUMO) on the central metal. Thus, as seen in Figures 1−4, the four-electron repulsion is minimized when the Ir(Cl)$(PH_3)_2$ lone pair (i.e., the HOMO) is directed away from the migrating halogen atom.

(26) Su, M.-D.; Chu, S.-Y. Manuscript in preparation.
(27) (a) Becke, A. D. *Phys. Rev. A* **1988**, *38*, 3098. (b) Lee, C.; Yang, W.; Parr, R. G. *Phys. Rev. B* **1988**, *37*, 785. (c) Becke, A. D. *J. Chem. Phys.* **1993**, *98*, 5648.
(28) Ricca, A.; Bauschlicher, C. W. *Theor. Chim. Acta* **1995**, *92*, 123.
(29) Hay, J. P.; Wadt, W. R. *J. Chem. Phys.* **1985**, *82*, 299.
(30) Hay, J. P.; Wadt, W. R. *J. Chem. Phys.* **1985**, *82*, 284.
(31) *Gaussian 94:* Frisch, M. J.; Trucks, G. W.; Schlegel H. B.; Gill, P. M. W.; Johnson, B. G.; Robb, J. R.; Cheeseman, J. R.; Keith, T.; Peterson, G. A.; Montgomery, J. A.; Raghavachari, K.; Al-Laham, M. A.; Zakrzewski, V. G.; Ortiz, J. V.; Foresman, J. B.; Cioslowski, J.; Stefanov, B. B.;

pseudopotential, with a standard LANL2DZ contraction.[31] For hydrogen and carbon atoms the double-ζ basis of Dunning−Huzinaga was used.[32] Moreover, the restricted B3LYP approach was used in this work to describe all the stationary points, except for the triplet states of reactants, which were described by unrestricted wave functions. Hence, all the B3LYP calculations are denoted by B3LYP/LANL2DZ.

Vibrational frequency calculations at the B3LYP/LANL2DZ level were used to characterize all stationary points as either minima (the number of imaginary frequencies (NIMAG = 0) or transition states (NIMAG = 1). Furthermore, four of the reactions that we have investigated (i.e., **SET2-TS-F**, **SET2-TS-Cl**, **SET2-TS-Br**, and **SET2-TS-I**) have been probed in some detail by determining the intrinsic reaction coordinate (IRC)[33] with the algorithm proposed by Schlegel.[34]

Acknowledgment. We are very thankful to the National Center for High-Performance Computing of Taiwan and the Computing Center at Tsing Hua University for generous amounts of computing time. We also thank the National Science Council of Taiwan for their financial support. We thank Professor H. B. Schlegel for providing useful software. We are grateful to one reviewer for critical comments on the paper.

JA9831148

Nanayakara, A.; Challacombe, M.; Peng, C. Y.; Ayala, P. Y.; Chen, W.; Wong, M. W.; Andres, J. L.; Replogle, E. S.; Gomperts, R.; Martin, R. L.; Fox, D. J.; Binkley, J. S.; Defrees, D. J.; Baker, J.; Stewart, J. P.; Head-Gordon, M.; Gonzalez, C.; Pople, J. A., Gaussian, Inc., Pittsburgh, PA, 1995.

(32) Dunning, T. H.; Hay, P. J. *Modern Theoretical Chemistry*; Schaefer, H. F., Ed.; Plenum: New York, 1976; pp 1−28.

(33) Fukui, K. *J. Phys. Chem.* **1970**, *74*, 4161.

(34) Gonzalez, C.; Schlegel, H. B. *J. Phys. Chem.* **1989**, *90*, 2154.